Central European Journal of Energetic Materials
ISSN 1733-7178; e-ISSN 2353-1843

Cent. Eur. J. Energ. Mater. 2024, *21*(4): 361-383; DOI 10.22211/cejem/195325
Article is available in PDF-format, in colour, at:
https://ipo.lukasiewicz.gov.pl/wydawnictwa/cejem-woluminy/vol-21-nr-4/

Research paper

Analyzing Safety Measures for Munitions under Different Logistic Configurations Incorporating Large Standard Shaped Charges

Muhammad Saqib Awan, Zheng Xiang Huang*), Xudong Zu, Qiang Qiang Xiao, Bin Ma
Nanjing University of Science and Technology, Jiangsu 210094, China
** E-mail:* huangyunjust@outlook.com

Abstract: In modern warfare, rocket-propelled grenades (RPGs) pose significant threats due to their widespread availability and effectiveness. However, research on safeguarding munitions transported in containers using palletized load systems against RPG attacks is limited. This study assesses the safety of munitions in both unprotected and protected container configurations using steel and ceramic add-on protections, with 56mm shaped charge munitions as the target. Experimental setups with 89 mm shaped charges comprised of COMPB explosive and copper liner were developed as RPG surrogates, alongside corresponding simulations using ANSYS AUTODYN. Aluminum buffer plates (75 mm thick) were added to meet RPG7 requirements. Safety evaluations for 56 mm JH-2 shaped charge munitions were conducted with standard and improved armor thicknesses. Results show significant damage from detonation when armor thickness was below 50 mm, but no detonation in one configuration with 50 mm steel armor, confirmed by simulations. This research highlights vulnerabilities and potential mitigations for munitions transported via palletized load systems facing RPG threats.

Keywords: palletized load system, munition safety assessment, shaped charge jet initiation, Lee- Tarver ignition and growth model, JH-2 explosive, RPG, composition B

1 Introduction

The secure transport of munitions is crucial for military operations. Container Express (CONEX) containers and their contemporary variations, celebrated for their durability, security features, and adaptability, have emerged as the cornerstone of modern military logistics [1] using a palletized load system. These containers routinely house a diverse arsenal, including mortars, artillery shells, and shaped-charge warheads for breaching armored vehicles and fortifications [2]. However, ensuring the integrity of these munitions within the confined space of a container, particularly against rocket-propelled grenade (RPG) attacks, remains a paramount concern for military effectiveness. The widespread use of CONEX containers stems from the 1952 invention by the US Army during the Korean War [3]. These standardized containers have since become ubiquitous in global trade and transportation. Recognizing logistical limitations in battlefield storage, Finnerty *et al.* [4] investigated the feasibility of CONEX containers as field storage facilities, driven by concerns regarding the safe containment of mortar rounds, illumination flares, and high-explosive munitions. Research by Hill [5] focused on munition cook-off within reinforced metal containers designed for transporting 155 mm artillery shells. These containers are equipped with reinforced steel walls that exceed the specifications established by the International Organization for Standardization (ISO). ISO containers, which evolved from the originally military-utilized CONEX containers, adhere to standardized dimensions and designs suitable for a wide range of commercial applications. Steyerer and Stange [6] explored mitigating sympathetic detonation between adjacent ISO containers used for munition storage in military camps by employing an earth-covering technique. Additionally, Madsen *et al.* [7] investigated the influence of sandbag formations on mitigating the impact of explosions on munitions stored within containers. Tobin *et al.* [8] focused on reinforced CONEX containers for storing TOW (Tube-launched, Optically-tracked, Wire-guided) missiles, incorporating significantly bolstered steel wall plates.

Despite these advancements, no research has addressed the vulnerability of munition-carrying CONEX containers to RPG attacks during transport. This gap in knowledge is concerning given the widespread use of RPGs in modern warfare. RPGs are man-portable, inexpensive, and easy to operate, making them a favored weapon of insurgents and terrorist groups [9]. Their simple design allows for easy proliferation and use by non-state actors. A typical RPG consists of a fuse, warhead, rocket motor, and stabilizer [10-12]. RPG warhead design has evolved, but a prevalent configuration involves a copper liner supported by high explosives, and a detonator encased in a steel cover [13]. Detonation of this

warhead creates a super-fast jet of molten metal capable of piercing even thick armor [14]. This destructive power makes RPGs a significant threat to lightly armored vehicles [15, 16] in the current work the warhead penetration capability was determined against more contemporary high-hardness (500 HB).

The effectiveness of RPGs against armored vehicles translates to a considerable threat against CONEX containers, especially considering RPG's potential use to replace rifles in modern warfare [17]. Moreover, their widespread deployment is exemplified by instances of RPG attacks on helicopters, including during takeoff, landing, and low-altitude flight [18]. Insurgent groups have exploited this weakness to devastating effect, as exemplified by the 1993 Somali attack where RPGs downed two US Black Hawk helicopters [19]. Besides, the evolution of RPGs has seen numerous advancements, ranging from the widely deployed RPG-7 to sophisticated models such as the RPG-30, capable of evading active protection systems deployed on main battle tanks [20]. Previous studies have indicated that the majority of munitions detonate when subjected to RPG-7 threat levels, with only select highly insensitive ordnance remaining intact [21].

Given the destructive power and widespread use of RPGs, it is evident that they present a significant threat to the transportation of munitions stored within CONEX containers. The potential ramifications of a successful RPG attack on a container carrying munitions are grave, including the risk of secondary explosions, dispersion of hazardous ordnance over a wide area, and the possibility of causing harm to both military personnel and civilians. However, research in this area is exceedingly limited. This research seeks to address this crucial gap in understanding by investigating the vulnerability of munitions stored within CONEX containers to RPG attacks. Our study aims to assess the effectiveness of various protective measures, such as add-on steel armor and ceramic materials, in mitigating the impact of RPG-7 attacks during transport. To accomplish this, we will produce standardized shaped charges to replicate the characteristics of the RPG-7 rocket-propelled grenade, utilizing the Held criteria, which quantifies jet energy based on the square of its velocity multiplied by the jet's diameter, as outlined by Baker *et al.* [22] with a v^2d value of 141 $mm^3/\mu s^2$ established for the RPG-7. In this study, the 56 mm JH-2 shaped charge will be employed as the target within the steel CONEX container. The experimental setup will involve the utilization of both standard container wall thickness and reinforced wall thickness, achieved by the installation of supplementary steel or ceramic materials in front of the attacking jet.

2 Experimental Insights into Munition Transport Safety

2.1 Development of 89 mm COMPB and 56 mm JH-2 target shaped charges

In this investigation, the safety of a 56 mm JH-2 target shaped charge was evaluated using an 89 mm shaped charge filled with COMPB explosive [23]. Shaped charges operate on a specific priciple, illustrated in Figures 1(a) and 1(b), which delineate the essential components, namely a detonator, the explosive (COMPB, 60 wt.% RDX and 40 wt.% TNT), and a copper metal liner. OFHC copper was chosen for the liner due to its demonstrated effectiveness in penetrating targets. The detonator's blast triggers a powerful shockwave within the explosive, which rapidly travels outward at the explosive's Chapman-Jouguet velocity. This shockwave then impacts the liner material, exerting pressure that forces it inward. This inward collapse effectively concentrates the explosion's energy, leading to the formation of a super-hot, high-speed jet of molten copper. Shaped charges are investigated because they play a pivotal role in modern munitions due to their ability to focus explosive energy with precision, maximizing destructive impact. Examples include anti-tank missiles like the TOW missile, which utilize shaped charges to penetrate armored vehicles. Similarly, the Rocket Propelled Grenade-7 (RPG-7) employs a shaped charge warhead for its anti-armor capabilities, demonstrating the versatility and effectiveness of this technology in military applications. In the present investigation, we aim to evaluate the safety parameters associated with the 56 mm JH-2 (95% RDX, 3% DNT and 2% CZ) shaped charge utilized as the target specimen during transportation within CONEX containers [24]. The dimensional specifications of the shaped charge are delineated in Figure 1(c) for reference and analysis.

2.2 Safety assessment set up configurations

The first step was to replicate the jet energy profile similar to that of an RPG-7 projectile, which was achieved by placing a 75 mm thick aluminum buffer plate was positioned 50 mm away from an 89 mm shaped charge This plate was not merely a passive obstacle but functioned as a regulator, fine-tuning the jet energy output of the shaped charge. By manipulating the interaction between the shaped charge and the buffer cylinder, it was possible to adjust the jet's energy level to mirror the specifications of an RPG-7 projectile.

In the second step the safety assessment of munitions transported within CONEX containers was conducted utilizing four distinct configurations denoted: 1, 2, 3 and 4. Configuration 1 involved solely the container itself, devoid of any supplementary protective measures. Within this setup, a 5 mm ammunition box

was employed to encase the 56 mm shaped charge and its associated 10 mm steel cover. It was assumed that the container wall possessed a thickness of 10 mm, acknowledging the common practice among military entities to modify container wall thicknesses relative to standard ISO containers. Configuration 2, as depicted in Figures 2(a) and 2(b), comprises a fortified 60 mm container wall oriented in the anticipated direction of a shaped charge assault. In contrast, Configuration 3 integrates 40 mm aluminum oxide ceramic material as supplementary armor, positioned with a clearance 10 mm between the container wall and ceramic material. The container wall has a thickness of 10 mm, while the ammunition box and the steel cover for the 56 mm shaped charge retain identical specifications as in preceding configurations. Configurations 1, 3 and 4 are shown in Figures 3(a), 3(b) and 3(c), respectively.

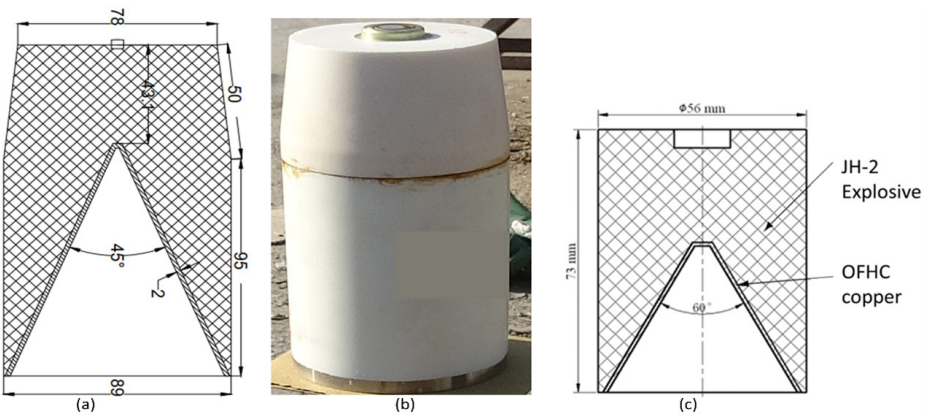

Figure 1. Dimensions of the 89 mm COMPB shaped charge (a), real image depicting the 89 mm COMPB shaped charge (b) and dimensions of 56 mm shaped charge used as target munition (c)

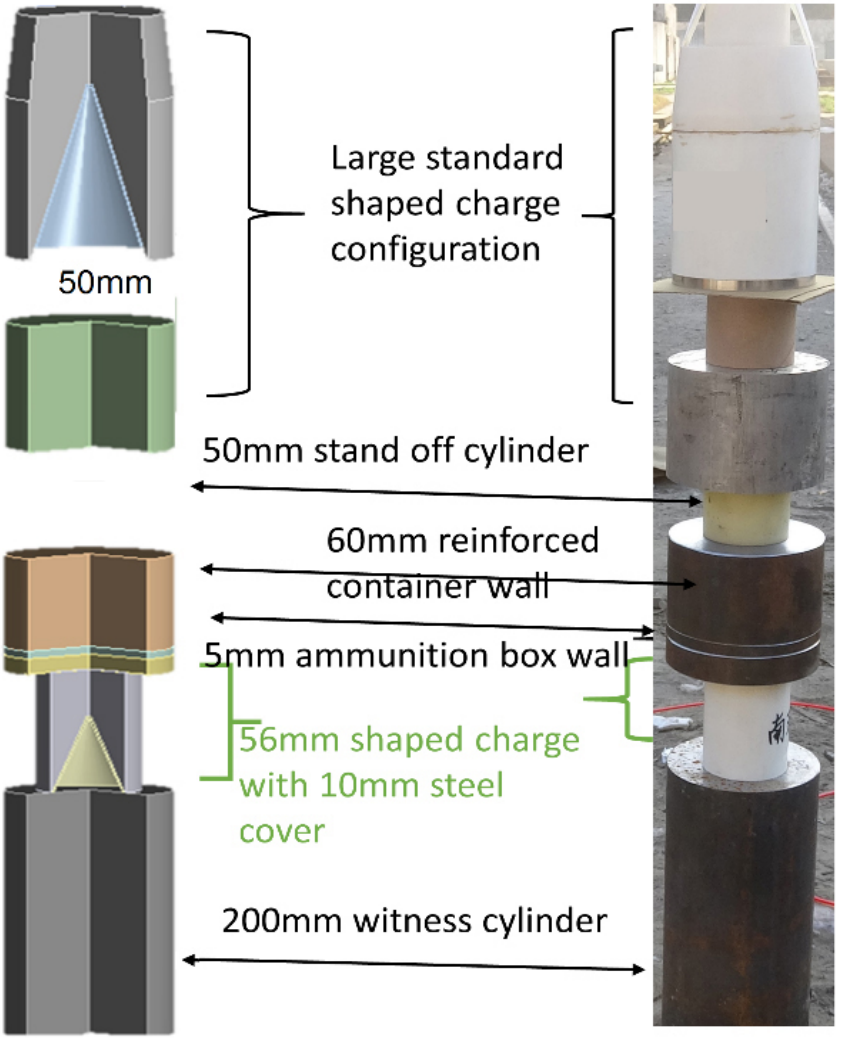

(a) (b)

Figure 2. Configuration 2 presented of a schematic (a) and in the real image (b), includes reinforced 50 mm steel protection attached to a 10 mm thick container, shown as a 60 mm steel cylinder along with steel ammunition box and cover

(a) (b) (c)

Figure 3. Images of: – Configuration 1, with only 10 mm outer steel container wall (a), – Configuration 3, which utilizes 40 mm ceramic addon protection (b), and Conifguration 4, which employes 40 mm steel protection at 10 mm gap from container 10 mm container wall (c)

Furthermore, Configuration 4 incorporates 40 mm steel additional armor, strategically positioned at a 10 mm distance from the CONEX container wall. The container wall has a thickness of 10 mm and ammunition box maintain a thickness of 5 mm, akin to previous iterations, while the thickness of the shaped charge cover has been increased to 20 mm.

3 Experimental Results and Analysis

3.1 High speed camera images

High-speed camera recordings were employed to investigate the detonation characteristics across all four configurations. Analysis of the high-speed footage reveals that within Configuration 1, the 56 mm shaped charge failed to withstand the detonation resulting from the attack of the standard 89 mm COMB shaped charge configuration. Notably, the 56 mm shaped charge initiated instantaneously, with subsequent examination confirming the instantaneous consumption of all explosive material involved in the detonation event. A visual representation of this detonation occurrence is provided in Figure 4.

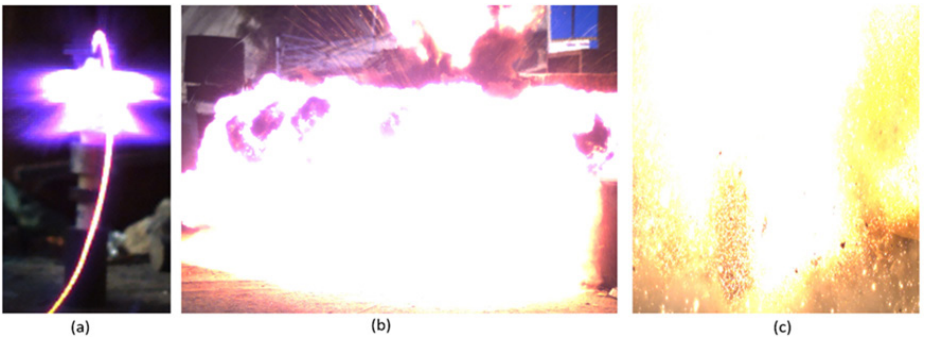

Figure 4. Illustration of Configuration 1 demonstrating the inability to ensure the safety of the 56 mm shaped charge during transportation *via* CONEX containers: the detonation of a large standard shaped charge (a, b) and the detonation event involving the 56 mm target shaped charge (c)

The high-speed camera analysis of Configuration 2 presents a distinct departure from the findings observed in Configuration 1. Specifically, Configuration 2 effectively prevented the detonation of the 56 mm target shaped charge. Instead, the recorded footage exclusively illustrates the combustion of

JH-2 explosive material. This stark disparity in detonation behavior between the two configurations is graphically depicted in Figure 5.

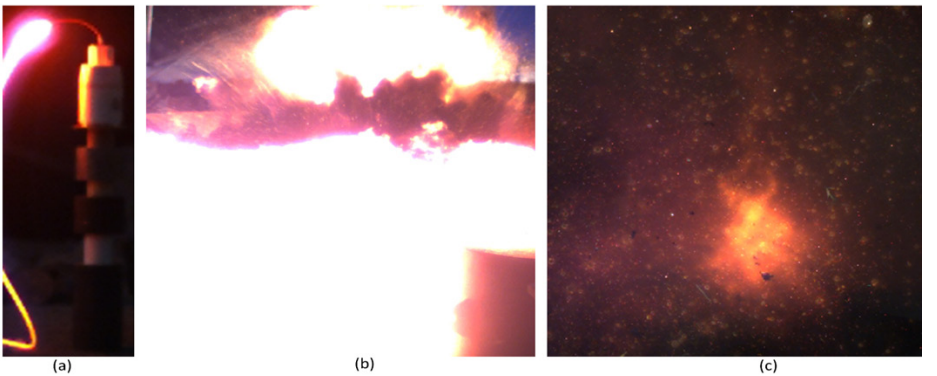

Figure 5. Illustration of Configuration 2 showcasing the protective efficacy of the 56 mm shaped charge during CONEX container transportation: the detonation of a large standard shaped charge (a, b) and exclusively displayed the combustion of the JH-2 explosive within the 56 mm shaped charge (c)

This deviation can be attributed to the substantial thickness of steel present in front of the 56 mm shaped charge. Notably, this steel barrier serves a dual function, it absorbs the energy of the attacking shaped charge jet and compresses the JH-2 explosive, thereby diminishing inherent hotspots within the explosive material and rendering it more homogenous. Consequently, this phenomenon engenders a decreased sensitivity of JH-2 explosive. Consequently, upon being struck by the shaped charge jet, the 56 mm target shaped charge's JH-2 explosive undergoes combustion instead of detonation.

Diverging from the outcomes observed in Configuration 2, Configuration 3, which integrated Al_2O_3 ceramic as additional protection for the CONEX container, failed to impede the detonation of the 56 mm target shaped charge upon being subjected to an assault by the large standard shaped charge configuration. This phenomenon is visually depicted through high-speed camera images presented in Figure 6. Configuration 4 incorporated a 40 mm supplementary steel layer positioned 10 mm away from the CONEX container, alongside a 5 mm thick container wall, a 5 mm thick ammunition box, and a sturdier 20 mm steel cover for the 56 mm shaped charge. Despite these measures, they proved insufficient to thwart the detonation of the 56 mm target shaped charge, as evidenced in Figure 7.

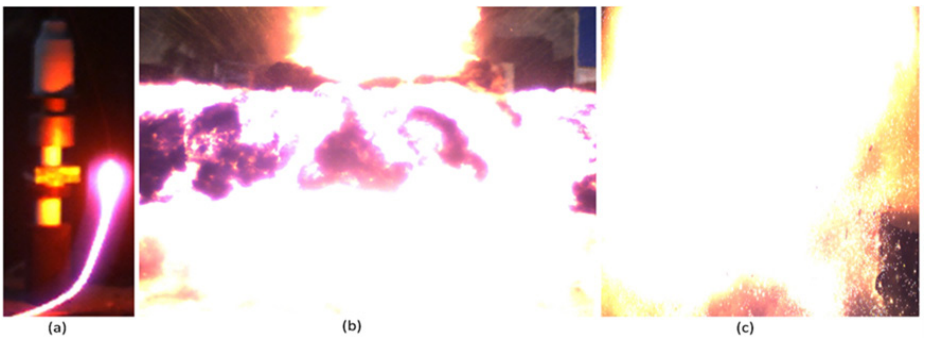

Figure 6. The depiction of Configuration 3 showcases its failure to guarantee the security of the 56 mm shaped charge while being transported in CONEX containers: the detonation caused by a large standard shaped charge (a, b) and the detonation of the 56 mm target shaped charge (c)

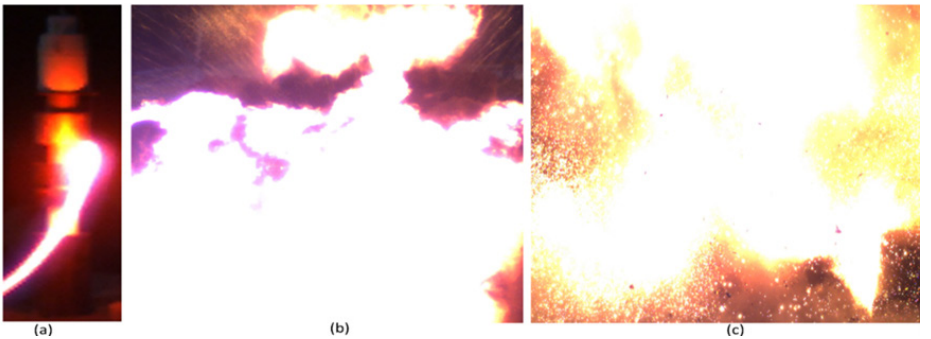

Figure 7. The portrayal of Configuration 4 reveals its inability to ensure the protection of the 56 mm shaped charge during transit within CONEX containers: the detonation initiated by a large standard shaped charge (a, b) and the detonation event involving the 56 mm target shaped charge (c)

3.2 Condition of the witness cylinder

In the first configuration, a shaped charge effectively penetrated a 75 mm-thick aluminum buffer cylinder, subsequently striking the container wall. It then penetrated a 5 mm-thick steel ammunition box before reaching the 10 mm-thick steel cover housing the JH-2 explosive, resulting in its detonation. Consequently, the witness cylinder sustained partial destruction, as illustrated in Figure 8(a). Conversely, in the second configuration, the shaped charge

first penetrated a 75 mm-thick aluminum buffer cylinder before encountering a 60 mm-thick additional steel protective layer. It then proceeded to penetrate a 5 mm-thick ammunition box and subsequently impacted a 10 mm-thick cover for the JH-2 56 mm-shaped charge. Notably, the shaped charge did not detonate in this configuration, meeting the safety criteria outlined in Allied Ordnance Publication 4526. This is corroborated by the intact condition of the witness cylinder, depicted in Figure 8(b). In Configuration 3, incorporating a 40 mm aluminum oxide ceramic material as additional protection prior to the 5 mm-thick container wall, the 56 mm-shaped charge successfully detonated within the 5 mm-thick steel ammunition box cover, encased by a 10 mm casing. This detonation is evidenced by the damage incurred by the steel witness cylinder, as depicted in Figure 8(c). Lastly, in the fourth configuration, wherein a 40 mm steel add-on protection was positioned at a 10 mm distance from the 5 mm-thick steel container wall, and the ammunition box featured the same 5 mm steel wall thickness, the cover for the JH-2 56 mm-shaped charge was increased to 20 mm. Despite these modifications, the 56 mm-shaped charge detonated, resulting in damage to the steel witness cylinder, as illustrated in Figure 8(d).

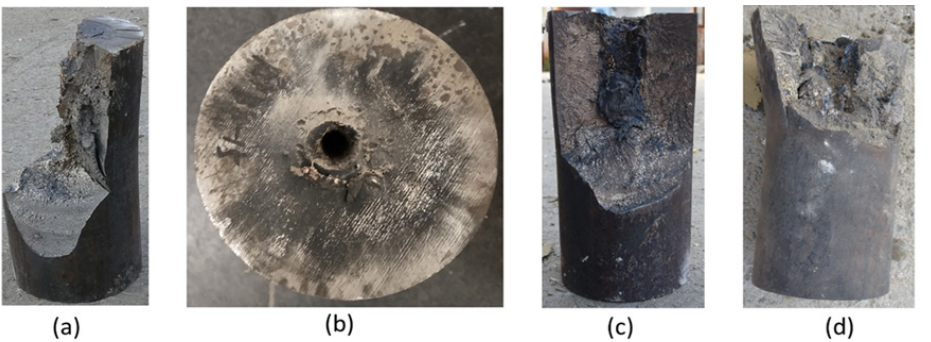

Figure 8. Evidence of the detonation of target 56 mm shaped charges for Configurations 1, 3, and 4, (a, c and d, respectively) and the illustration of the safety of munition in Configuration 2 (d)

4 Numerical Analysis

4.1 Modeling

This research utilized computer simulations to assess the effects of standard shaped charge jets (SCJs) on various explosive safety configurations for CONEX containers. The software employed for this purpose was ANSYS AUTODYN,

a program adept at simulating nonlinear dynamic behavior. This approach enabled a detailed comparison between the predicted explosive response level of JH-2 explosives and real-world observations obtained through experimentation. The simulations specifically relied on the Lee-Tarver ignition and growth (IG) model to capture the behavior of the explosive material in response to the overdriven shocks generated by the SCJ impact. It's important to note that due to inherent limitations within the IG model, modeling procedure employed a uniform unit system comprising centimeters, grams, and microseconds [25] rather than the usual SI units. The explosive material and the liner were meshed elements within the computational domain and the mechanism for forming the jet was captured utilizing Eulerian framework of AUTODYN. The computational domain, consisting of 20 nodes per centimeter, was demarcated by establishing outflow boundaries at its edges to minimize undesired reflections during shockwave propagation. The surrounding environment was simulated as air, with predefined values for internal energy measured at 2.06640×10^5 J/kg and density at 0.001225 kg/m^3 [26]. In simulating the pivotal phase of jet perforation within different cylinders, AUTODYN's Lagrangian solver was utilized to ensure simulation stability [27]. Additionally, AUTODYN's erosion capability played a pivotal role in maintaining accuracy by preserving suitable time steps during the simulation, essential for precision and error prevention. As noted by Li *et al.* [28], the incorporation of both the Lagrangian solver and erosion capability ensures the accuracy of the entire simulation endeavor by rectifying extensively distorted mesh elements. Jet velocity was quantified using jet profile plot data as well as gauge points embedded at appropriate points within the computational domain.

4.2 Material parameters and constitutive equations

The numerical investigation of shaped charge performance requires accurate material models for both the explosive and target materials. The study utilized a simulation technique that integrated the well-known equation of state (EOS) for explosives, namely Jones-Wilkins-Lee (JWL) EOS, with high explosive burn (HEB) method to model the COMPB explosive [29]. This approach provides a well-established framework for capturing the detonation behavior of explosives within computational simulations. The JWL EOS is a widely employed equation for describing the pressure-volume-energy relationship in high explosives [30]. As expressed by Lee *et al.*, the JWL EOS can be mathematically represented by Equation 1.

$$P = A\left(1 - \frac{\omega}{R_1}\right)e^{-R_1 V} + B\left(1 - \frac{\omega}{R_2 V}\right)e^{-R_2 V} + \frac{\omega E}{V} \tag{1}$$

where P represents pressure, V denotes relative volume (V/V_0), E signifies internal energy per unit mass, and V_0 is initial specific volume. The coefficients R_1, A, R_2, ω, and B are material-specific constants that calibrate the equation to match the explosive's unique properties. Table 1 summarizes the JWL EOS coefficients obtained for the COMPB explosive used in this study. Additionally, the table includes CJ velocity (D) of COMPB, which is a crucial parameter for characterizing the explosive's detonation characteristics.

Table 1. JWL COMPB explosive parameters

R_1	R_2	Density [g/cm^3]	D [cm/μs]	A [Mbar]	B [Mbar]	ω
4.2	1.1	1.717	0.7980	5.2423	0.07678	0.34

A critical aspect of safety assessment according to allied ordnance publication 4526 is capturing the response level of the target explosive. The IG model was selected as the method in this study to simulate how explosives respond to jet attacks generated by shaped charges [31]. IG model utilizes JWL-EOS to model the material properties of both explosive and its detonation products. The Lee-Tarver IG model incorporates separate terms for ignition and growth processes. The ignition term mathematically represents generation and consequent ignition of hot spots within explosive material. Initially, the reaction progresses slowly due to the burning of isolated hot spots, as reflected by the first growth term. However, once these localized areas of high temperature amalgamate, the second growth factor addresses the swift escalation of the reaction toward its culmination [32]. Equation 2 mathematically expresses the Lee-Tarver IG model formulation.

$$\frac{dF}{dt} = I(1-F)^b(\eta_s - 1 - a)^x + G_1(1-F)^c\alpha^d P^y + G_2(1-F)^e\alpha^g P^z \qquad (2)$$

where η_s represents the relative density of the unreacted explosive, defined as "ρ_s/ρ_0" where ρ_s is current and ρ_0 is initial explosive density, respectively. Pressure and mass fraction of the explosive are denoted by P and F, respectively. The remaining variables (z, g, e, G_1, G_2, a, b, x, c, d, y and I) are constants specific to the explosive material being modeled. A crucial parameter within the IGM model is the critical compression parameter "a." This value signifies the threshold level of compression that must be achieved before the ignition and reaction processes can commence. Mathematically, this is represented by the condition $\eta_s \geq 1 + a$. Only when the relative density of the unreacted explosive reaches or exceeds this critical value will the reaction be triggered. Tables 2 and 3 provide the Lee-

Tarver IGM model parameters for JH-2 explosive used in this study.

Table 2. Unreacted JWL JH-2 EOS parameters

E_o [Gerg/mm]	R_1	R_2	Density [g/cm^3]	A [Mbar]	B [Mbar]	ω
0.00090	11.3	1.13	1.717	310	0.0328	0.8938

Extensive studies have revealed that for a broad range of heterogeneous explosives, several IGM parameters exhibit consistent values. These parameters (*a, b, c, d, e* and *z*) are primarily associated with the underlying geometry of the hot spots formed during the initial stages of the reaction. Their consistent values suggest a less pronounced dependence on the specific explosive material. In contrast, other IGM parameters exhibit a stronger dependence on the explosive being modeled. These parameters include the initiation term constant *(I)* and the exponent *(x)* within the ignition term. These parameters are sensitive to factors like shock wave intensity and duration. Furthermore, four growth parameters *(G_1, y, G_2* and *z)* also demonstrate variations across different explosives. These parameters govern the rate and progression of the reaction after ignition has been triggered. Table 3 summarizes the Lee-Tarver IGM reaction rate parameters employed in this study for the JH-2 explosives. It is important to note that the JWL EOS parameters for both the unreacted and reacted explosive states were obtained from the work of Xiao-wen Hong *et al.* which can be referenced for further details on JWL parameter selection [24].

Table 3. Lee Tarver IGM parameters for JH-2 explosive

G_1	G_2	I	a	b	c	x	y	z	e	d	g
140	1000	4×10^6	0.022	0.667	0.667	7	2	3	0.067	0.329	0.333

Numerical simulations of shaped charge performance require accurate material models to capture the behavior of the target, liner, and any intermediate materials like buffer plates. This study adopts a combined approach for material modeling. The steel target, aluminum buffer plate, and copper liner characteristics are represented using a shock EOS. This approach relates the internal energy and pressure of a material under high-pressure conditions, encompassing both regions inside and outside the Hugoniot curve. To account for the material strength effects within these components, the Johnson-Cook strength model is employed. This widely used constitutive model incorporates factors like strain hardening, strain rate sensitivity, and temperature dependence to describe the material's resistance to deformation and eventual failure. By combining the shock EOS with the Johnson-Cook strength model, the simulations can capture both the pressure-volume

relationship and the material's strength under the dynamic loading conditions encountered during a shaped charge attack. The shock EOS and the Johnson-Cook model are mathematically represented by Equations 3 and 4, respectively.

$$P = P_H + \rho\Gamma(e - e_H) \tag{3}$$

$$\sigma_y = (A + B\varepsilon_p^n)(1 + Clog\varepsilon_p^*)(1 - T_H^m) \tag{4}$$

The normalized plastic strain rate, denoted as ε^*_p, and the dynamic behavior of yield stress described by σ_y are significant factors in understanding the material's response. Additionally, the effective plastic strain, ε_p, plays a crucial role. Together with these parameters, Equation 4 identifies the static yield stress as A, the hardening constant as B, and C serves as the representation for the strain rate constant. Thermal softening and hardening are characterized by the exponents m and n, respectively. The relative melting temperature, denoted as T_m^H, and the shear modulus, G, along with other pertinent parameters of the strength model, are presented in Table 4, the values taken from Xu *et al.* [33]. Al_2O_3 parameters were directly taken from AUTODYN material library.

Table 4. Aluminum, steel 45 and copper Johnson-Cook parameters

Metal	T_m [K]	A [GPa]	G [GPa]	m	B [GPa]	n	C	Γ	ρ [g/cm^3]
Copper	1356	0.09	46	1	0.29	0.31	0.025	2	8.96
Aluminum	1220	0.04	27.10	1.03	0.292	0.27	0.01	1.97	2.7
Steel 45	1793	0.79	81.80	1.09	0.51	0.26	0.014	2.17	7.83

4.3 Simulation and modeling results

The experimental measurement of the jet energy level for the large 89 mm shaped charge was deemed impractical and hazardous, necessitating reliance solely on numerical simulation. Drawing from our prior investigation employing smaller shaped charges, wherein our numerical model reliably predicted experimental outcomes, we applied the same computational approach in this study. Consequently, our analysis reveals that the jet energy level corresponds to that of the RPG-7 post-penetration of a 75 mm aluminum buffer plate, as illustrated in the accompanying Figure 9 [34, 35]. Notably, the shaped charge jet's velocity measures 5.596 mm/μs, with a diameter of 4.5 mm, resulting in an approximate v^2d value of 140.9 mm^3/μs^2.

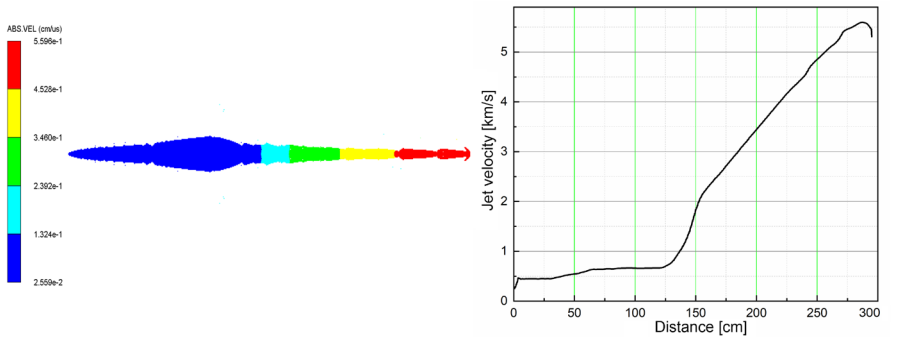

(a) (b)

Figure 9. Velocity contours of shaped charge jet post 75 mm aluminum buffer cylinder penetration (a) and velocity profile of jet, and its energy level same as RPG7, measured at a v^2d value of 140.9 mm^3/μs^2 (b)

In Configuration 1, our inquiry centered on a standard CONEX container featuring a 10 mm wall thickness, supplemented by a 5 mm ammunition box steel and a 10 mm steel cover placed in front of the 56 mm JH-2 shaped charge, devoid of any additional metal or ceramic reinforcement prior to the container wall. Regrettably, this arrangement proved inadequate in halting the detonation of the 56 mm target shaped charge. Our computational scrutiny corroborates empirical findings, affirming an instantaneous detonation as illustrated by pressure contours in Figure 10(a). Configuration 2, entailing the incorporation of a substantial 55 mm steel protective layer encompassing the 5 mm steel container wall, 5 mm ammunition box, and 10 mm steel cover akin to Configuration 1, was investigated next. During experiments, the container wall and 55 mm steel protection functioned as a unified entity. Encouragingly, the 56 mm JH-2 shaped charge did not undergo detonation under these conditions, as demonstrated by Figure 10(b). Figure 10(c) presents the corresponding pressure contour illustration for Configuration 3, providing compelling evidence affirming the occurrence of detonation of the 56 mm shaped charge jet. Notably, in Figure 10(d), a discernible pattern analogous to the detonation observed in Configuration 3 is evident for Configuration 4, as depicted by pressure contours in Figure 10(d).

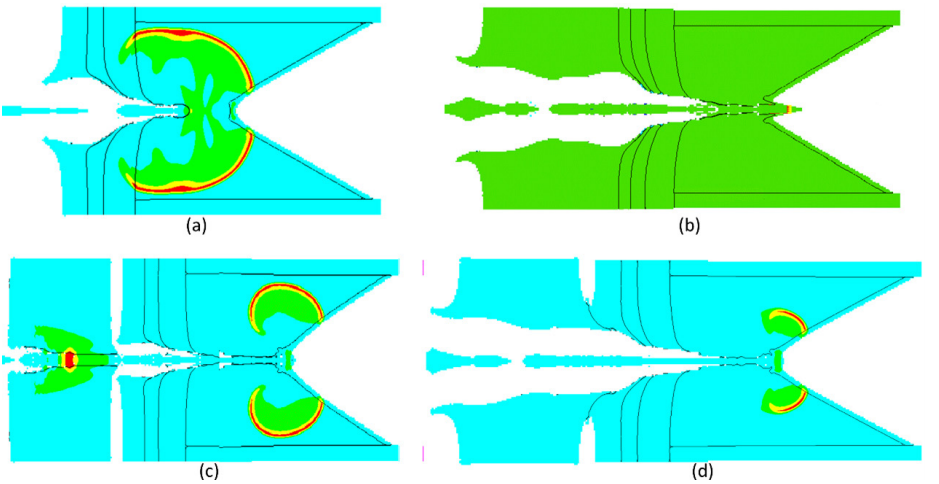

Figure 10. Pressure contours for: – Configuration 1 shows prompt detonation (a), – Configuration 2 display no detonation, aligning with experimental results (b), – Configuration 3 exhibits bow shock detonation (c) and – Configuration 4 demonstrates late-stage detonation, suggesting increased steel protection for enhanced safety (d)

Further analysis of density and pressure profiles within the 56 mm target-shaped charge also confirms the detonation of the 56 mm shaped charge in Configuration 1, as depicted in Figure 11. According to the ignition and growth model for the reaction initiation, the compression induced by the shaped charge jet must exceed a critical compression value defined as $(1 + a)$. For the JH-2 explosive, this critical compression is calculated to be 1.022. Thus, if the JH-2 explosive within the 56 mm shaped charge is compressed to 1.022 times or greater than its initial density, ignition will occur. Inspection of Figure 10(a) reveals that the density of JH-2 has been compressed to $\rho_f = 2.28$ g/cm^3, surpassing its initial density of $\rho_i = 1.717$ g/cm^3. Consequently, JH-2 is compressed to 1.31 times its initial density, significantly exceeding the critical compression threshold of $(1 + a) = 1.022$, thereby confirming its ignition which then led to prompt detonation, as already evident in Figure 10(a). Additional evidence is presented in Figure 11(b), where the pressure of the shock wave produced, reaching 342 kbar in the explosive, exceeds the Chapman-Jouguet pressure of the JH-2 explosive, which is 295 kbar.

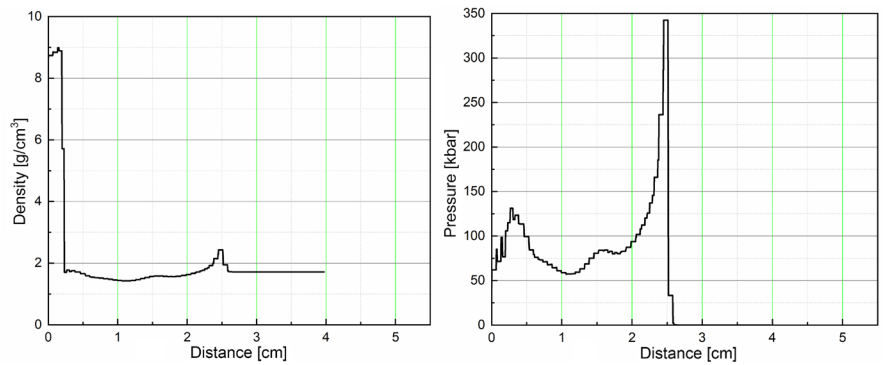

(a) (b)

Figure 11. Density profile indicates a compression of 1.31 times the initial density, greater than the critical compression of 1.022 required for detonation (a) and pressure profile also evidences detonation because of greater pressure generation than Chapman-Jouguet pressure for JH-2 explosive which is 295 kbar (b)

The density and pressure profile graphs for Configuration 2 provide additional validation that JH-2 explosive detonation did not occur in this scenario. In this case, the maximum density reached a value of 1.75. Consequently, this resulted in a compression ratio of 1.019, which falls short of the critical compression threshold of 1.022 required for ignition to start. As a result, no reaction occurred in the case of Configuration 2. Moreover, the pressure profile indicates a minimal generation of pressure within the 56 mm shaped charge, significantly lower than its Chapman-Jouguet pressure. These findings collectively reinforce the conclusion that detonation did not occur under these conditions, as shown in Figure 12.

Additionally, the pressure and density profiles for Configurations 3 and 4 are somewhat similar as both configurations undergo a penetrative detonation at a later stage, this behavior of pressure and density is depicted in Figure 13, which further corroborates the experimental observation for Configuration 3 and 4 confirming the later detonation event in Configurations 3 and 4. This agreement of simulation and experimental data strengthens the understanding of the detonation process within these specific configurations.

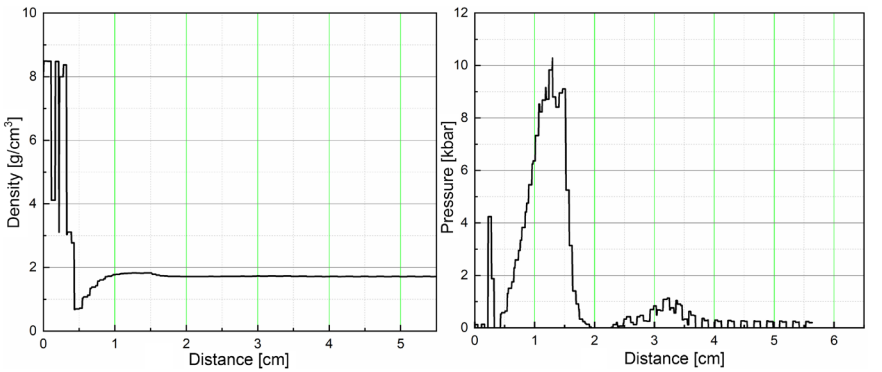

(a) (b)

Figure 12. Density profile indicate a compression of only 1.019 times the initial density, falling short of the critical compression of 1.022 required for ignition (a) and pressure profile indicates no detonation, *i.e.* results are significantly lower than the Chapman-Jouguet pressure (b)

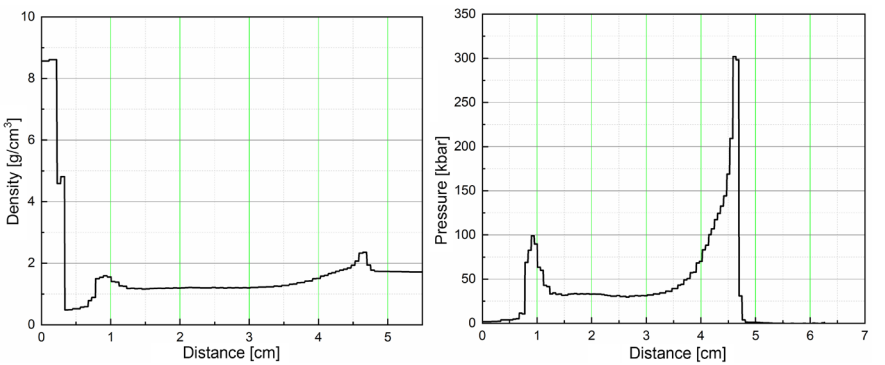

(a) (b)

Figure 13. Density profile indicates a compression of 1.28 times the initial density, greater than the critical compression of 1.022 required for ignition (a) and pressure profile evidences detonation because of greater pressure generation than Chapman-Jouguet pressure for JH-2 explosive which is 295 kbar (b)

5 Conclusions

This research addresses the pressing issue of safeguarding munitions transported in containers using palletized load systems against RPG attacks. Through experimental setups and simulations, we assessed the safety of both unprotected and protected container configurations utilizing steel and ceramic add-on protections, with 56 mm shaped charge munitions as target. This study sheds light on the vulnerabilities inherent in munition transport systems facing RPG threats and emphasizes the importance of adequate protective measures. Moving forward, our insights offer valuable guidance for enhancing the security of munitions during transportation in modern warfare scenarios. The important points are as follows.

- Experimental development of an RPG-7 surrogate configuration was achieved using an 89 mm shaped charge with COMPB explosive and a 2 mm thick copper liner, alongside a 75 mm buffer plate positioned 50 mm away. Simulation results revealed a jet energy level, indicated by its v^2d value, closely matching that of an RPG-7.
- Commercial containers typically range from 1.6 to 4 mm in thickness, while military-grade containers may have thicker walls. However, our study demonstrated that a 10 mm thick container wall is insufficient to prevent explosive detonation within the container.
- A combination of a 10 mm steel container wall and an additional 50 mm steel add-on protection proved effective in preventing detonation of a 56 mm shaped charge in an improved safety configuration.
- A 10 mm steel container wall along with additional add-on protection consisting of 40 mm aluminum oxide ceramic or 40 mm steel resulted in bow shock detonation of the 56 mm shaped charge in separate cases.
- These findings underscore the critical importance of appropriate container and add-on protection thicknesses in mitigating the detonation risk of explosive munitions during transportation.

Conflicts of Interest

The authors declare that there are no conflicts of interest regarding the publication of this paper.

Acknowledgements

Financial support for this research was provided by the National Natural Science Foundation of China (Grant Nos. 11972196,11872214).

References

[1] Nussbaumer, P. Lethality-Model for HD 1.2/1.4 Ammunition Debris Throw Due to An Explosion on a Vehicle. *Proc. 34th DoD Explosives Safety Semin.,* Portland, US-OR, **2010**.

[2] Lawrence, W. Test Data on the Storage of Mixed Munitions in Conex Containers. *Proc. 24th DoD Explosive Safety Semin*., St. Louis, US-MO, **1990**.

[3] DiMoia, J.P. Reconfiguring Transport Infrastructure in Post-War Asia: Mapping South Korean Container Ports, 1952-1978. *Hist. Technol.* **2020**, *36*(3-4): 382-399; https://doi.org/10.1080/07341512.2020.1862990.

[4] Finnerty, A.E.; Watson, J.L.; Peregino II, P.J. A Safer Method of Storing Ammunition in a Conex Container. *Proc. 25th Explosives Safety Semin.,* Anaheim, US-CA, **1992**, Vol. 1, pp. 163-181.

[5] Hill, D.B. Propagation and Fire Tests Conducted on a Secondary Steel Container Designed for Movement of Chemical Agent Artillery Projectiles. *Proc. 24th DoD Explosive Safety Semin*., St. Louis, US-MO, **1990**.

[6] Steyerer, M.; Stange, O. DEU Ammunition Storage in Earth Covered ISO-Containers. *Proc. 34th DDESB Semin*., US-OR, **2010**.

[7] Madsen, N.K.; Madsen, S.H.; Thomsen, A.J. Concept of Field Storage of Ammunition and Explosives in 20'Standard Container. *Proc. 26th DoD Explosive Safety Semin*., Miami, US-FL, **1994**.

[8] Tobin, T.M.; Rossi, R.A. The U.S. Army Safeload Explosives Safety Program. *Proc. 25th Explosives Safety Semin.,* Anaheim, US-CA, **1992**, Vol. 1, pp. 133-149.

[9] Coghe, F. Efficiency of Different Cage Armour Systems. *Appl. Sci.* **2022**, *12*(10) paper 5064; https://doi.org/10.3390/app12105064.

[10] Niezgoda, T.; Panowicz, R.; Sybilski, K.; Barnat, W. Numerical Analysis of Missile Impact being Shot by Rocket Propelled Grenades with Rod Armour. *WIT Trans. Modell. Simul.* **2011**, *51:* 625-633; https://doi.org/10.2495/CMEM11055.

[11] Shuker, S.T. Rocket-Propelled Grenade Maxillofacial Injuries and Management. *J. Oral Maxillofac. Surg.* **2006**, *64(*3): 503-510; https://doi.org/10.1016/j.joms.2005.11.033.

[12] Sehirlioglu, A.; Komurcu, M.; Ozturk, C.; Oguz, E.; Atesalp, A.S.; Altinmakas, M. An Unexploded Rocket-Propelled Grenade in the Thigh. *Eur. J. Orthop. Surg. Traumatol.* **2008**, *18*(3): 233-236; https://doi.org/10.1007/s00590-007-0292-3.

[13] Babu, V.; Vunnam, M. Comparative Analysis of Arbitrary Lagrange in Eulerian (ALE) and Adaptive Smooth Particles Hydrodynamics (SPH) Simulation of Rocket Propelled Grenade (RPG) on Armors. *Proc. 31st Int. Symp. Ballistics*, Hyderabad, India, **2019**.

[14] Fayed, A.I.H.; Abo El Amaim, Y.A.; Elgohary, D.H. Investigating the Behavior of Manufactured Rocket Propelled Grenade (RPG) Armour Net Screens from Different Types of High Performance Fibers. *Int. J. Sci. Res.* **2019**, *8*(5): 2088-2091.

[15] Żochowski, P.; Podgórzak, P. Numerical Analysis of Effectiveness for Vehicle Net Systems Protecting Against Shaped Charge Projectiles. *Issues Armament Technol.*

2016, 139(3): 23-37; https://doi.org/10.5604/01.3001.0010.0533.
[16] Żochowski, P.; Warchoł, R.; Miszczak, M.; Nita, M.; Pankowski, Z.; Bajkowski, M. Experimental and Numerical Study on the PG-7VM Warhead Performance against High-Hardness Armor Steel. *Materials* **2021**, *14*(11) paper 3020; https://doi.org/10.3390/ma14113020.
[17] Yew, Y.Z. *How Can Rocket Launchers Replace Assault Rifles as the Standard Infantry Weapon?* Report FN 401, St. Jospeh's Institution, **2015**.
[18] Law, N.G. *Integrated Helicopter Survivability.* Doctoral Thesis, Cranfield University, UK, **2011**.
[19] Anderson, D.; Thomson, D. Analyzing Helicopter Evasive Maneuver Effectiveness Against Rocket-Propelled Grenades. *J. Guid. Control. Dyn.* **2014**, *37*(1): 277-289; http://dx.doi.org/10.2514/1.59318.
[20] Wallace, M. *BeHinD THe nUMBerS.*
[21] Arnold, W.; Rottenkolber, E. High Explosive Initiation Behavior by Shaped Charge Jet Impacts. *Procedia Eng.* **2013**, *58*: 184-193; https://doi.org/10.1016/j.proeng.2013.05.022.
[22] Baker, E.L.; Pham, J.; Madsen, T.; Poulos, W.; Fuchs, B.E. Shaped Charge Jet Characterization and Initiation Test Configuration for IM Threat Testing. *Procedia Eng.* **2013**, *58*: 58-67; https://doi.org/10.1016/j.proeng.2013.05.009.
[23] Hobbs, M.L.; Kaneshige, M.J.; Anderson, M.U. Cookoff of a Melt-Castable Explosive (Comp-B). *Proc. 27th JANNAF Propulsion Systems Hazards Joint Subcommittee Meeting*, Monterrey, CA, **2012**.
[24] Hong, X.W.; Li, W.B.; Cheng, W.; Li, W.B.; Xu, H.Y. Numerical Simulation of the Blast Wave of a Multilayer Composite Charge. *Def. Technol.* **2020**, *16*(1): 96-106; https://doi.org/10.1016/j.dt.2019.04.007.
[25] Zhang, X.F.; Huang, Z.X.; Qiao, L. Detonation Wave Propagation in Double-layer Cylindrical High Explosive Charges. *Propellants Explos., Pyrotech.* **2011**, *36*(3): 210-218; https://doi.org/10.1002/prep.201000004.
[26] Elshenawy, T.; Li, Q.M. Influences of Target Strength and Confinement on the Penetration Depth of an Oil Well Perforator. *Int. J. Impact Eng.* **2013**, *54*: 130-137; https://doi.org/10.1016/j.ijimpeng.2012.10.010.
[27] AUTODYN Theory Manual, Revision 4.0. Century Dynamics Inc., **1998**.
[28] Li, X.D.; Yang, Y.S.; Lv, S.T. A Numerical Study on the Disturbance of Explosive Reactive Armors to Jet Penetration. *Def. Technol.* **2014**, *10*(1): 66-75; https://doi.org/10.1016/j.dt.2014.01.006.
[29] Downes, D.; Bouamoul, A.; Ensan, M.N. *Numerical Simulation of the Shaped Charge.* Project DRDC-RDDC-2014-P38, Canada, **2014**.
[30] Lee, E.L.; Hornig, H.C.; Kury, J.W. *Adiabatic Expansion of High Explosive Detonation Products.* University of California, Lawrence Radiation Laboratory, Report UCRL-50422, Livermore, US-CA, **1968**.
[31] Lee, E.L.; Tarver, C.M. Phenomenological Model of Shock Initiation in Heterogeneous Explosives. *Phys. Fluids* **1980**, *23*(12): 2362-2372; https://doi.org/10.1063/1.862940.

[32] Souers, P.C.; Garza, R.; Vitello, P. Ignition and Growth and JWL++ Detonation Models in Coarse Zones. *Propellants Explos., Pyrotech*. **2002**, *27*(2): 62-71; https://doi.org/10.1002/1521-4087(200204)27:2<62::AID-PREP62>3.0.CO;2-5.
[33] Xu, W.; Wang, C.; Chen, D. Formation of a Bore-Center Annular Shaped Charge and Its Penetration into Steel Targets. *Int. J. Impact Eng.* **2019**, *127*: 122-134; https://doi.org/10.1016/j.ijimpeng.2019.01.008.
[34] Awan, M.S.; Huang, Z.; Zu, X.; Xiao, Q.; Ma, B. Application of Lee-Tarver Model for Energetic Materials Safety Assessment Utilized in Aerospace Applications. *Aerosp.* **2024**, *11*(7) paper 513; https://doi.org/10.3390/aerospace11070513.
[35] Awan, M.S.; Huang, Z.X.; Zu, X.; Xiao, Q.Q.; Bin, M. Safety Assessment of Insensitive and Conventional Energetic Materials using 50 mm Small Standard Shaped Charges: Numerical and Experimental Insights. *Lat. Am. J. Solids Struct.* **2024**, *21*(3) paper e540; https://doi.org/10.1590/1679-78258054.

Contribution

Muhammad Saqib Awan:	foundations, methods
Zheng Xiang Huang:	conception
Xudong Zu:	performing the experimental part
Qiang Qiang Xiao:	performing statistical analysis
Bin Ma:	other contribution to the publication

Received: May 9, 2024
Revised: October 28, 2024
First published online: November 25, 2024